Published in final edited form as:

FASEB J. 2023 May ; 37(5): e22908. doi:10.1096/fj.202201848R.

Disrupted intercellular bridges and spermatogenesis in fatty acyl-CoA reductase 1 knockout mice: A new model of ether lipid deficiency

Bo Pan[1], **Shuo Yuan**[1,2], **Linda Mayernik**[3], **Yi Tian Yap**[1], **Kamiar Moin**[3], **Charles S. Chung**[1], **Krishnarao Maddipati**[4], **Stephen A. Krawetz**[5,6], **Zhibing Zhang**[1,5], **Rex A. Hess**[7], **Xuequn Chen**[1]

[1]Department of Physiology, Wayne State University, School of Medicine, Detroit, Michigan, USA

[2]Department of Occupational and Environmental Medicine, School of Public Health, Wuhan University of Science and Technology, Wuhan, Hubei, China

[3]Department of Pharmacology, Wayne State University, School of Medicine, Detroit, Michigan, USA

[4]Department of Pathology, Wayne State University, School of Medicine, Detroit, Michigan, USA

[5]Department of Obstetrics & Gynecology, Wayne State University, Detroit, Michigan, USA

[6]Center for Molecular Medicine and Genetics, School of Medicine, Wayne State University, Detroit, Michigan, USA

[7]Comparative Biosciences, College of Veterinary Medicine, University of Illinois Urbana-Champaign, Urbana, Illinois, USA

Abstract

Peroxisomal fatty acyl-CoA reductase 1 (FAR1) is a rate-limiting enzyme for ether lipid (EL) synthesis. Gene mutations in FAR1 cause a rare human disease. Furthermore, altered EL homeostasis has also been associated with various prevalent human diseases. Despite their importance in human health, the exact cellular functions of FAR1 and EL are not well-understood. Here, we report the generation and initial characterization of the first Far1 knockout (KO) mouse model. Far1 KO mice were subviable and displayed growth retardation. The adult KO male

Correspondence: Xuequn Chen, Department of Physiology, Wayne State University, School of Medicine, Detroit, MI, 48201, USA. xchen@med.wayne.edu.

AUTHOR CONTRIBUTIONS

Bo Pan, Zhibing Zhang, and Xuequn Chen designed the studies; Krishnarao Maddipati developed LC–MS method; Bo Pan, Shuo Yuan, Linda Mayernik, Yi Tian Yap, Kamiar Moin, Zhibing Zhang, and Rex A. Hess acquired data; Bo Pan, Charles S. Chung, Krishnarao Maddipati, Stephen A. Krawetz, Zhibing Zhang, Rex A. Hess, and Xuequn Chen performed data analysis and prepared figures; Bo Pan, Linda Mayernik, Krishnarao Maddipati, Stephen A. Krawetz, Zhibing Zhang, Rex A. Hess, and Xuequn Chen wrote or edited the manuscript. All authors read and approved the final paper.

DISCLOSURES

The authors declare no conflict of interest.

ETHICS STATEMENT

The study does not involve human subjects, human tissue, or human data. All mice studies were approved by the Institutional Animal Care and Use Committee of Wayne State University.

SUPPORTING INFORMATION

Additional supporting information can be found online in the Supporting Information section at the end of this article.

mice had smaller testes and were infertile. H&E and immunofluorescent staining showed fewer germ cells in seminiferous tubules. Round spermatids were present but no elongated spermatids or spermatozoa were observed, suggesting a spermatogenesis arrest at this stage. Large multi-nucleated giant cells (MGC) were found lining the lumen of seminiferous tubules with many of them undergoing apoptosis. The immunofluorescent signal of TEX14, an essential component of intercellular bridges (ICB) between developing germ cells, was greatly reduced and mislocalized in KO testis, suggesting the disrupted ICBs as an underlying cause of MGC formation. Integrative analysis of our total testis RNA-sequencing results and published single-cell RNA-sequencing data unveiled cell type-specific molecular alterations underlying the spermatogenesis arrest. Many genes essential for late germ cell development showed dramatic downregulation, whereas genes essential for extracellular matrix dynamics and cell–cell interactions were among the most upregulated genes. Together, this work identified the cell type-specific requirement of ELs in spermatogenesis and suggested a critical role of Far1/ELs in the formation/maintenance of ICB during meiosis.

Keywords

ether lipids; fatty acyl-CoA reductase 1; intercellular bridge; RNA sequencing; spermatogenesis

1 | INTRODUCTION

Ether lipids (ELs) are glycerophospholipids with a characteristic ether bond at the sn-1 position of the glycerol backbone, where a fatty alcohol is attached. In contrast, fatty acids are attached via ester bonds at both the sn-1 and sn-2 positions in diacyl phospholipids.[1–3] This biochemical difference in ELs has profound structural and functional implications and their biosynthesis requires a specialized pathway involving the concerted action of multiple organelles. The first few steps of this pathway take place in peroxisomes. Peroxisomal enzymes, dihydroxyacetone phosphate acyltransferase (GNPAT), and alkyl-dihydroxyacetone phosphate synthase (AGPS) are needed to generate the ether bond, while fatty acyl-CoA reductase (FAR) is required to supply the fatty alcohols by reducing fatty acyl-CoAs. The resulting precursor, alkyl-dihydroxyacetone phosphate, is shuttled across the peroxisomal membrane to the endoplasmic reticulum (ER) where subsequent enzymatic steps are completed.[1–4]

Illustrating the importance of ELs in human physiology, mutations in peroxisomal genes essential in the EL biosynthesis pathway can result in a human EL deficiency disease, called rhizomelic chondrodysplasia punctata (RCDP). Examples include PEX7 (peroxisomal biogenesis factor 7), GNPAT, AGPS, FAR1, and PEX5l, leading to RCDP1, RCDP2, RCDP3, RCDP4, and RCDP5, respectively.[5] EL deficiency not only can lead to rare human genetic disorders like RCDPs but also has been associated with common human diseases such as Alzheimer's disease and obesity.[3,6–8] Very recently, ELs have been linked to cancer cell ferroptosis.[9,10] In past years, PEX7, GNPAT, and AGPS knockout mouse models were generated and studied.[11–16] These EL-deficient mouse models share a common defect, male infertility due to disrupted spermatogenesis.

Male fertility reflects the temporal and spatial effects of genetic and environmental factors throughout spermatogenesis that starts with the mitotic division of the spermatogonial stem cells. Subsequently in meiosis I, one primary spermatocyte divides into two secondary spermatocytes, each of which divides into two haploid spermatids in meiosis II. Through spermiogenesis, these round spermatids undergo maturation accompanied by elongation and then spermiation or disengagement release into the lumen as spermatozoa.[17–21] The interactions of germ cells with Sertoli cells also play a crucial role in their differentiation into mature sperm.[22] In this highly specialized process, one unique and crucial feature is the formation of permanent stabilized intercellular bridges (ICB) during germ cell cytokinesis, which connect clonal daughter germ cells in a highly organized syncytium, for the hypothesized purpose of exchanging cytoplasmic components and synchronization of the step-wise processes of spermiogenesis.[23,24] Intercellular bridges are evolutionarily conserved from invertebrates to humans and are essential for spermatogenesis and male fertility.[25,26]

Mammalian fatty alcohol synthesis is accomplished by two fatty acyl-CoA reductases, FAR1 and FAR2. These two isozymes have different substrate specificities and tissue distributions. While Far1 was detected in many mouse tissues, Far2 was found with a more restricted tissue distribution.[27,28] Far1 has been reported to function as a rate-limiting enzyme in the EL synthesis pathway and undergoes rigorous regulations.[29–32] Despite its importance in EL biosynthesis and human diseases, a Far1 knockout mouse model has not been studied. Here, we report a Far1 knockout mouse model generated by CRISPR/Cas9 gene-editing and initial characterization of the male phenotype, the disrupted spermatogenesis. In this work, the cell type-specific and stage-specific requirements of ELs in spermatogenesis were identified and a critical role for Far1 and ELs in ICB formation during meiosis was uncovered. This study also helps to provide insight into how a specific class of lipids may play an essential role in spermatogenesis.

2 | MATERIALS AND METHODS

2.1 | Mice and genotyping

Far1 whole-body knockout mice, Far1$^{em1(IMPC)Wtsi}$, were produced in C57BL/6N genetic background using the CRISPR/Cas9 mediated exon deletion. Heterozygous Far1 knockout mouse founders were obtained from Wellcome Trust Sanger Institute and bred in the university animal facility. The offspring were studied. Before weaning, genomic DNA was prepared from tail biopsy using DirectPCR Lysis Reagent (Mouse Tail) (Viagen Biotech), and mouse genotyping was done through PCR analysis using the following primers: P1 (CCATAGCTTTGTACATAATCTTGTTGT), P2 (CCAAGCCTCTAACACATGGA), and P3 (ACTGGACAGCATCTCTGCAA). PCR analyses were performed following a standard procedure and PCR products were analyzed by agarose gel electrophoresis. If not otherwise specified, adult male mice at 4 months of age were used in different studies.

2.2 | Protein extraction and western blot analyses

The total proteins were extracted from testis tissue in lysis buffer supplemented with the Halt™ protease inhibitors cocktail and the protein concentrations were determined using

BCA protein assay (Thermo Scientific). Protein samples were separated on NuPAGE 4%–12% Bis-Tris precast mini gels from Invitrogen. The separated proteins were then transferred onto a nitrocellulose membrane. For western blotting, the membranes were incubated with the following primary antibodies overnight at 4°C: rabbit anti-Far1 (Thermo Fisher; 1:500), anti-GAPDH (Sigma-Aldrich; 1:1000), goat anti-Wnt4 (Novus Biologicals; 1: 1000), anti-Timp1 (Novus Biologicals; 1:1000), anti-Tnp1 (Proteintech, 1:1000), and anti-Tnp2 (Santa Cruz, 1:1000). The secondary antibodies bound to the nitrocellulose membrane were then detected using enhanced chemiluminescence reagents (GE Healthcare) and then digitally imaged using the ChemiDoc™ MP Imaging System (Bio-Rad).

2.3 | Lipid sample preparation and targeted LC–MS analysis of ether lipids in the testis

Tissues were homogenized using zirconium beads and a high-frequency oscillator (Precellys) in phosphate-buffered saline (PBS) pH 7.2 at a ratio of 9:1 (buffer to tissue by weight). Homogenate containing about 2 mg protein was supplemented with deuterated internal standards (100 ng each of pPC 18:0/18:1-d9 and pPE 18:0/18:1-d9) and total lipids were extracted using methyl tert-butyl ether.[33] The extracted lipids were analyzed by LC–MS for plasmalogens PC, and plasmalogens PE using targeted analysis as described earlier[34] using a QTRAP5500 mass analyzer (Sciex).

2.4 | Sperm counting and tissue histology

Sperm counting and tissue histology were performed as previously described.[35] Briefly, the cauda epididymis was immediately removed from each mouse after euthanasia and placed in 1 mL of warm PBS solution at 37°C. Two openings were cut in each epididymis to release sperm. Sperm were collected and fixed with 4% formaldehyde for 10 min at room temperature. Sperm number was counted using a hemocytometer chamber under a light microscope. For histology analysis, testis and cauda epididymis of adult mice were fixed in 4% formaldehyde for 24 h prior to embedding in paraffin wax. The tissues were sectioned at 5 μm thickness on glass slides and then stained with hematoxylin and eosin using the H&E Staining Kit (Abcam). Images were taken as described previously.[35]

2.5 | Immunofluorescence staining, TUNEL assay, and confocal microscopy

To prepare frozen tissue blocks for immunofluorescent staining, the testis was cut into two halves and fixed in 4% paraformaldehyde for 24 h at room temperature. The fixed tissues were then placed in Tissue-Tek™ molds and embedded in Tissue-Tek™ O.C.T. compound. Frozen testis blocks were sectioned on a cryostat at 8 μm thickness and then tissue sections were transferred onto Superfrost™ Plus microscope slides. Tissues were washed three times for 5 min with PBS, incubated with 0.1 M lysine in PBS for at least 30 min, and blocked with 5% BSA for 2 h at room temperature. Primary antibodies were added to the specimen and incubated in a moisture chamber overnight at 4°C. The following primary antibodies were used: anti-SCP3 (Abcam; 1:400), anti-DAZL (Abcam; 1:100), anti-TEX14 (Abcam; 1:2000), and anti-vimentin (Biolegend; 1:3000). In addition, fluorescent Alexa Fluor conjugate of lectin PNA (ThermoFisher Scientific; 1:400) was also used. Appropriate secondary antibodies were incubated for 1 h at room temperature. Then the stained sections were mounted using ProLong™ Diamond Antifade Mountant with DAPI (Invitrogen) prior to confocal imaging analyses. Terminal Deoxynucleotidyl Transferase dUTP Nick

End Labeling (TUNEL) assays were performed using an in situ DNA fragmentation assay kit (BioVision) following the manufacturer's instructions. Briefly, testicular tissue sections were incubated with the TUNEL staining solution (10 μL TdT reaction buffer, 0.75 μL TdT enzyme, 8 μL FITC-dUTP, 32.25 μL DdH2O) for 60 min at 37°C. The stained sections were then analyzed by fluorescence microscopy (apoptotic cells showing green fluorescent staining over an orange-red Propidium Iodide counter-staining). The fluorescence-stained testis sections were visualized and imaged in Microscopy, Imaging, and Cytometry Resources (MICR) Core using a Zeiss LSM 780 confocal equipped with a Zeiss Axio Examiner.Z1 upright microscope with fixed stage. Fluorophores were detected with a 405 nm diode laser, a 458/488/514 nm multi-line Argon laser, and a 561 nm HeNe laser utilizing 10×, 20×, 40× oil, and 63× oil objectives. Acquisition settings were kept constant across similar experiments.

2.6 | RNA sequencing and bioinformatics analysis

Seminiferous tubules were harvested from testis and stored in RNAlater solution (ThermoFisher). Total RNAs from three wild type and three KO mice were isolated using Qiagen RNeasy Plus Mini Kit (Qiagen). RNA sequencing and initial data analysis were performed at Admera Health (South Plainfield, NJ). Briefly, isolated RNA sample quality was assessed by High Sensitivity RNA Tapestation (Agilent Technologies) and quantified by Qubit 2.0 RNA HS assay (ThermoFisher). Library was constructed by using Truseq Stranded Total RNA kit (Illumina) with poly-A selection. Final libraries quantity was assessed by Qubit 2.0 (ThermoFisher) and quality was assessed by TapeStation D1000 ScreenTape (Agilent Technologies). The average final library size was about 330 bp with an insert size of about 200 bp. Illumina® 8-nt dual indices were used. Equimolar pooling of libraries was performed based on QC values and sequenced on an Illumina® Novaseq S4 (Illumina) with a read length configuration of 150 PE for 40 M PE reads per sample (20 M in each direction). DESeq2 software package was used for differential expression analysis and GOATOOLS was used to analyze pathway enrichment.

2.7 | Statistical methods

All continuous variables are presented as mean ± SEM unless indicated otherwise. Differences between the two groups were evaluated for statistical significance with a 2-tailed unpaired *t*-test. When the difference among the three groups was evaluated, 1-way ANOVA followed by the Tukey test for pairwise comparisons was performed. A p-value <.05 is considered statistically significant.

3 | RESULTS

3.1 | Generation and validation of the Far1 knockout mice

Far1 whole-body knockout mice were produced from lines originating from CRISPR zygote microinjection using the CRISPR/Cas9 gene-editing technology. Four sgRNAs were used to target the 5′ and 3′ intronic flanking regions thereby deleting Far1 exon 5 on chromosome 7 (Figure 1A). Three primers were designed for genotyping and Sanger Sequencing to confirm the deletion (Figure 1A). A 475 bp deletion was identified that confirmed the CRISPR/Cas9-mediated domain disruption including the deletion of the entire exon 5. Using the

allele-specific primers and the end-point PCR analyses, genotypes could be unambiguously determined by the unique PCR product sizes in the wild-type (WT), heterozygous, and homozygous (referred to as KO hereafter) mice (Figure 1B). As expected, WT mice showed two PCR bands at ~695 and ~287 bp respectively. In contrast, only one band, at ~220 bp, was detected in the KO mice, and three bands in the heterozygous mice.

To verify the lack of Far1 protein expression in Far1$^{-/-}$ mice, western blot (WB) analysis with testis extracts was carried out using a Far1-specific antibody. As shown in Figure 1C, Far1 proteins were present, with strong signals and predicted molecular weight (~59 kDa), in both the WT and heterozygous mice, but were not detected in the KO mice. To confirm that the loss of Far1 protein led to enzymatic deficiency, ether lipid levels were analyzed by LC–MS in the WT and KO mouse testis. It was found that the levels of ether-linked phosphatidylcholines (pPC), as well as ether-linked phosphatidylethanolamines (pPE) were essentially eliminated in the KO testis (Figure 1D,E). Together, these results confirmed the development of a Far1 KO mouse model, which is ether lipid deficient.

The Far1 KO mice were subviable with a marked variability in lifespans. The majority, over 70%, of the expected homozygous pups died embryonically or perinatally. The remaining KO mice that passed a critical stage before weaning were able to survive like their WT and heterozygous littermates. Among the 618 mice genotyped at weaning, the genotype distribution was plotted for the females (Figure 2A), the males (Figure 2B), or the total (Figure 2C) separately. The observed frequency of wild-type, heterozygous, or homozygous genotype in all mice was around 39%, 54%, and 7%, respectively. The survived Far1 KO mice displayed growth retardation. At birth, Far1 KO pups appeared indistinguishable from their WT littermates, but throughout development, they weighted significantly less than their WT and heterozygous littermates. The growth curves of the female or male mice between 4 and 12 weeks of age were shown in each genotype (Figure 2D,E).

3.2 | Male infertility, testicular abnormalities, and disrupted spermatogenesis

The adult Far1 KO male mice were infertile. When compared to the WT controls, the Far1 KO testes appeared smaller in size (Figure 3A) and weighed significantly less (Figure 3B). Cauda epididymal mature sperm were obtained from the epididymis and counted. Normal sperm numbers were found in WT and heterozygote males, but no sperm were found in the KO males (Figure 3C). In the representative bright field images, mature and healthy-looking sperm from WT mice were shown (Figure 3D *left*). In contrast, only round, likely degenerative residual bodies or sloughed germ cells, were observed in the KO mice (Figure 3D *right*). Consistent with these findings, the H&E staining showed that mature sperm filled the lumen of the WT epididymis (Figure 3E *left*). However, no sperm were observed in the KO epididymal lumen (Figure 3E *right*). Of note, the large multinucleated giant cells observed in the testes of KO males (Figure 4B) were absent in the epididymal lumen (Figure 3E), which may be due to the narrow diameter (30–50 μm) of the common efferent duct and initial segment epididymal lumens.[36–38]

In the H&E staining of testis sections, the seminiferous tubules of the wild-type mice showed normal structure, with evidence of all stages of spermatogenesis (Figure 4A). However, seminiferous tubules in KO mice contained significantly fewer cells (Figure 4B),

with no elongated spermatids or spermatozoa being present in the seminiferous epithelium. The absence of normal spermatids and mature sperm suggested that spermatogenesis was arrested at an earlier stage. The remaining layers of germ cells also displayed various degrees of disorganization (Figure 4B). In addition, very large multi-nucleated giant cells (MGCs, highlighted with arrows) were found in the Far1 KO but not in WT tubules (Figure 4B). The MGCs, some larger than 50 μm in diameter, were found lining the lumen of the seminiferous tubules and consisted of numerous round spermatids, many of which were undergoing apoptosis as detected by TUNEL staining (green cells in Figure 4C *right*). It is worth noting that there were still significant numbers of TUNEL-negative MGCs present in the seminiferous tubules (red cells in Figure 4C *right*). In contrast to the KO mice, very few TUNEL-positive cells were found in the WT seminiferous tubules (Figure 4C *left*). Moreover, these green-stained cells were mainly found at the base of the WT seminiferous tubules, consistent with some spermatogonial germ cell apoptosis occurring during normal spermatogenesis.[39] A significant and quantitative increase was observed in the numbers of TUNEL-positive apoptotic cells per seminiferous tubule in the Far1 KO testes compared to the WT testes (Figure 4D *left*). Similarly, a significant increase was observed in the percentage of TUNEL-positive seminiferous tubules in the Far1 KO testes (Figure 4D *right*).

3.3 | Cell type- and stage-specific defect of spermatogenesis in Far1 KO testes

To understand cell-type-specific defects of spermatogenesis in ELs deficient Far1 KO testes, we performed detailed immunofluorescent staining studies using specific markers for spermatogonia, spermatocytes, spermatids, and Sertoli cells respectively. Peanut agglutinin (PNA), a plant lectin protein, is widely used as a sperm acrosome-specific marker. In the testis sections, PNA staining appeared as donut- or crescent-shaped in WT seminiferous tubules, highlighting the presence of various stages of round spermatids and elongating spermatids (Figure 5A, top panels, and 5B *left*). In contrast, in KO seminiferous tubules, PNA staining appeared as small punctate dots in the germ cell layers and as large bright clusters within the MGCs at the lumen (Figure 5A, bottom panels, and 5B *right*). These changes indicated a spermatogenesis arrest at the round spermatid stages which was consistent with the histology finding in Figure 4B. Synaptonemal complex protein 3 (SCP3) is a component of the synaptonemal complex formed during the prophase of meiosis in spermatocytes. As shown in Figure 5C, SCP3 staining marked spermatocytes near the basement in the seminiferous tubules of both WT and KO testes. This is similar to the staining we observed for the deleted azoospermia-like (DAZL), a RNA-binding protein essential for spermatogenesis (Figure 5D). In the WT seminiferous tubules, DAZL immunofluorescent signals marked spermatogonia at the basement, spermatocytes near the basement, and, to a lesser extent, the spermatids near the lumen. In the KO seminiferous tubules, however, some of the DAZL-positive (also SCP3-positive) spermatocytes became disorganized and were found near the lumen. In contrast, DAZL-positive (SCP3 negative) spermatogonia remained at the basement membrane and showed no dramatic change. In addition, punctate DAZL signals were found in the MGCs in the lumen of the KO seminiferous tubules.

To characterize the cell type- and stage-specific molecular alterations underlying the spermatogenesis arrest in Far1 KO testes, WT and KO testes RNAs were isolated and

sequenced. As shown in Table S1, among the 39 408 genes detected, 14 900 genes showed significant changes in the KO testes ($p < .01$), in which 1805 genes were downregulated with log2(fold changes) <−2 and 1019 genes were upregulated with log2(fold changes) >2. Such a large percentage of differentially expressed genes is consistent with the dramatically altered cellular compositions in the KO seminiferous tubules. Indeed, Gene Ontology (GO) analyses of the differentially expressed genes showed that among the top 10 most downregulated GO biological processes (Figure 6A), the vast majority of them, if not all, were related to spermatid differentiation, sperm motility, and fertilization. Consistently, among the top 10 most downregulated GO cellular components (Figure 6B), many were sperm components including 9 + 2 motile cilium, flagellum, fibrous sheath, and acrosomal vesicle. These unique gene expression signatures elucidated the molecular basis of the spermatogenesis defect in the Far1 KO testis, namely a spermatogenesis arrest at the round spermatids with a complete absence of elongating spermatids and spermatozoa. This finding was further confirmed by comparing our results with the specific markers published in recent single-cell RNA-Seq studies.[40–43] Particularly, using the major cell type markers and germ cell cluster markers defined in a comprehensive roadmap of mouse spermatogenesis,[41] we calculated the means of the log2(fold changes) of these markers in our RNA-Seq results (Table S1) and unveiled the cell type-specific (Figure 6C) and stage-specific (Figure 6D) spermatogenesis defect in the Far1 KO testis. There was a significant reduction of round spermatid-specific gene expression and a dramatic suppression of elongated spermatid gene expression in the Far1 KO testis. These findings strongly supported a spermatogenesis arrest at the round spermatid in the KO testis which led to the loss of elongated spermatids and sperm. After the loss of late-stage germ cells, the gene expressions of the Leydig cells, Sertoli cells, and spermatogonia-specific markers were modestly increased in the KO testis (Figure 6C) (Table S1). To uncover the most upregulated genes, we focused on the genes with base Means >100 counts and log2(fold changes) >3.0. 37 genes were identified with Wnt4 showing the biggest increase, log2(fold change) >7.0, in the Far1 KO testis (Table S1). Among these most upregulated genes, many are essential for extracellular matrix dynamics and cell–cell interactions during germ-cell migration and differentiation. These genes included metalloproteinase inhibitor (Timp1), serine peptidase inhibitors (Serpina3n, Serpina3i), integrins (Itga5), and receptors (Tnfrsf12a) (Figure 6E) (Table S1). Western blot analysis confirmed the dramatically increased protein expressions of Wnt4 and Timp1 in the Far1 KO testis (Figure 6G). On the other hand, among the most downregulated genes were those essential for spermiogenesis including spermatid nuclear transition protein 1 (Tnp1), nuclear transition protein 2 (Tnp2), sperm protamine P1 (Prm1), and sperm protamine P2 (Prm2) (Figure 6F) (Table S1). Western blot analysis also confirmed the dramatic reduction of Tnp1 and Tnp2 protein expressions in the Far1 KO testis (Figure 6H).

3.4 | Disrupted intercellular bridge formation—A potential mechanism underlying the spermatogenesis arrest in ether lipid deficient testis

In somatic cell divisions, cytokinesis is the final process through which one cell is completely separated into two daughter cells. Germ cell cytokinesis, however, is a special form of cytokinesis in which cytokinetic abscission is blocked and a stable intercellular bridge (ICB) is formed to permanently connect the cytoplasm of the daughter cells in a syncytium. Mammalian germ cell ICBs include general cytokinesis components and

additional germ cell–specific factors such as TEX14 which is essential to block the terminal steps of abscission.[44] To better define the cellular and molecular defects underlying the MGC formation and spermatogenesis arrest in Far1 KO testes, we examined ICB formation using TEX14 immunostaining. As shown in Figure 7A, in the WT testis, Tex14 displayed a punctate staining between the germ cells in the seminiferous tubules, indicating the presence of ICBs. At higher magnification (Figure 7B), TEX14 signals were enhanced in areas connecting between spermatogonia, spermatocytes, or round spermatids. Frequently, small circles of TEX14 staining can be seen as a hallmark of ICB, a ring-like structure. In contrast to the WT controls, very few punctate TEX14 immunofluorescent signals were detected in the KO seminiferous tubules (Figure 7A,C), indicating defective ICB formation/stabilization in the absence of Far1 and ELs. Interestingly, despite an overall reduction of punctate TEX14 immunofluorescence, patchy Tex14 staining was observed on the multinucleated giant cell membrane in Far1 KO testis. Two separate examples are shown in Figure 7C,D (white arrows) indicating a disrupted localization of TEX14 in the KO testis. In contrast to the drastic changes observed in the germ cell ICBs, Sertoli cells, stained with the vimentin marker, showed very little change in the KO testis (Figure 7A–C red). It is worth noting that there were a few Sertoli cells found disorganized in some seminiferous tubules of the KO testis (Figure 7C). It is important that the dramatic reduction of TEX14 puncta was not primarily due to the reduction in germ cell numbers because the TEX14 puncta per nucleus was reduced by more than 50% in the KO seminiferous tubules (Figure 7E). These findings suggested that Far1 and ELs are required for the correct targeting of ICB proteins and male germ cell ICB formation/stabilization. A summary of spermatogenesis deficiencies in Far1 KO testis is shown in Figure 7F.

4 | DISCUSSION

In sperm plasma membranes, approximately two-thirds of the phosphoglycerolipids are ether-linked,[15] however, the physiological role of these lipids in the testis is not well-understood. Recent evidence showed that EL levels are highly regulated and Far1 is the major site for such regulation in the EL biosynthetic pathway.[29,32,45] In this study, we report the generation and initial characterization of the first Far1 knockout mice. The defective spermatogenesis phenotype revealed in our new EL deficiency mouse model is consistent with previous reports from other EL-deficient mouse models, including the Pex7 KO,[11] GNPAT KO,[12] the hypomorphic AGPS mutation mice,[13] and the AGPS deficient mice.[14] Although common histological defects were observed in these EL-deficient mouse models, a detailed molecular characterization of the disrupted spermatogenesis was lacking in previous studies, and the potential molecular mechanisms underlying the abnormality were poorly understood.

By comparing total testis RNA-Seq results with the single-cell RNA-Seq study,[41] the present study provided, in a cell type-specific and stage-specific manner, a molecular signature of the disrupted spermatogenesis in EL-deficient mouse testis. In general, the current molecular findings are consistent with our morphological observations and previous reports.[12–15] In contrast to the dramatic germ cell loss, the Leydig and Sertoli cells were much less affected. However, a potential effect of Far1 KO on the ectoplasmic specialization components cannot be ruled out, because it appears that disruption in the peroxisome functions and EL synthesis

in testicular germ cells, not only induced multinucleated germ cell formation, but also could impair the tight junctional complex.[46,47] A dynamic modulation of tight and adhesion junctions is essential for Sertoli-germ cell interactions during germ-cell maturation.[22] In Far1 KO testis, multiple genes essential in this process were among the most upregulated genes. These genes included Wnt4, Timp1, Serpina3n, Serpina3i, Itga5, and Tnfrsf12a. Wnt4 is a secreted protein essential for female sex determination and needs to be repressed for testicular development.[48–51] Recent results also indicated that Wnt4 repression was important for germ cell survival in adult testis.[52] Our findings suggested a dysregulation of extracellular matrix dynamics and Sertoli-germ cell interactions in Far1 KO testis. Future investigation is warranted using conditional Far1 KO in specific cell types, to determine if this impairment is one of the causes or consequences of germ cell loss in EL-deficient testis.

Helping to understand a potential mechanism underlying the MGC formation and spermatogenesis arrest in EL deficiency, another key finding in this study was the disruption of ICBs in Far1 KO testis. Stable ICB formation is a specific modification of somatic cytokinesis in germ cells. Therefore, the ICBs contain both general cytokinesis complexes, such as the mitotic kinesin-like protein 1 (MKLP1)-Male germ cell Rac GTPase-activating protein (MgcRacGAP) complex, as well as germ cell-specific factors including TEX14.[26] Centrosome protein 55 kDa, CEP55, is another key player localized to ICB.[53] Although the specific immunofluorescent signals of TEX14, an ICB marker, were drastically reduced and mislocalized in Far1 KO testis, it is not surprising that there were major differences between the Tex14 KO and Far1 KO mice. In the Far1 KO testes, meiosis occurred and round spermatids were formed; however, MGCs were formed by the opening of the ICBs between the newly formed spermatids. In contrast, testes of the Tex14 KO mice showed no formation of any type of spermatid and lacked MGC formation, because TEX14 has a role in blocking cell abscission at the final stage of cytokinesis. In the absence of TEX14, the cytoplasm of the male germ cells is completely separated after mitosis, causing spermatogenesis arrest before the completion of the first meiotic division.[44] Another important regulator of ICB formation is MgcRacGAP, a general cytokinesis factor that is located at the ICB.[54] In the germ cell conditional MgcRacGAP knockout testis, MGCs were observed in the PLZF+ spermatogonial cells but these were small compared to the round spermatid MGCs in the Far1 KO testis. Thus, MgcRacGAP deletion had a broader defect, interfering with germ cell cytokinesis and ICB formation at an earlier step than that seen in the Tex14 KO. Another factor that interacts with Rho/Rac is citron kinase and its deletion also resulted in spermatogonial MGC formation, with subsequent germ cell apoptosis.[55]

The Far1 KO phenotype suggests a role for ELs in regulating cytokinesis in a general manner, rather than specifically regulating TEX14. Our results suggest that Far1 and ELs are specifically required in germ-cell meiotic cytokinesis. A similar stage-specific requirement in germ cell cytokinesis was found for syntaxin 2 (STX2), an essential player in abscission.[56] In the STX2 nonsense mutant, as well as the KO mice,[57–59] STX2 deficiency disrupted ICBs and produced multinucleated spermatocytes. Interestingly, in both STX2 mutant and Far1 KO testes, TEX14 was found on the MGC membrane in an aberrant patchy pattern,[58] indicating a defective ICB protein complex assembly and targeting. Similarly, multinucleated spermatocytes lacking ICB structures were observed in mice with a conditional KO of EXOC1, a member of the Exocyst complex.[59] In male fruit

flies, mutations in conserved cytokinesis genes prevented normal ring canal formation, the alternate name of ICB in *Drosophila*, and created multinucleated germ cells.[60–62] These multinucleated cells developed into multinucleated spermatids. In rats, disruption of the actin ring by cytochalasin D also resulted in the formation of multinucleated spermatids.[63] These defects share even more similarities with the phenotype of our Far1 KO mice as well as the other EL-deficient mouse models.[12–15] Taken together, our results suggest a critical role for Far1 and ELs in ICB formation and/or stabilization during meiosis and the disrupted ICB underlying the MGC formation as one of the reasons for the massive germ cell loss in EL deficiency. The mechanistic details of this new function of Far1 and ELs warrant future investigation.

In addition to ELs, other classes of special lipids also play important roles in stabilizing meiotic germ cell ICBs. For example, loss of elongation of very long chain fatty acids protein 2 or germ cell-specific loss of either ceramide synthase 3 or glucosylceramide synthase, all led to MGC formation and spermatogenesis arrest in mice.[64,65] In the KO mice lacking key enzymes for seminolipids synthesis, spermatogenesis was arrested at the late pachytene stage.[66,67] ELs are chemically distinct from their diacyl counterparts, resulting in their unique structural and functional characteristics. Studies from in vitro and in vivo models suggested a variety of important biological functions of ELs including endogenous antioxidants, key components of GPI-anchors, facilitator of membrane fusion, organizers of the lipid raft microdomains, mediators of cell signaling,[2,68] and very recently, regulators of ferroptosis.[9,10,69] In the testis, our results indicated that the roles of Far1 and ELs in spermatogenesis are likely to be multifaceted (Figure 7F). An early step requiring ELs could be the stage-specific, dynamic regulation of ICB formation where ELs are needed to acquire the membrane curvature and/or to define a specific membrane domain for ICB-specific protein-targeting. It is also possible that Far1 and ELs are required for the vesicular transport of essential molecules to ICBs. It is important in future studies to tease out, using in vivo models as well as in vitro systems, how ELs coordinate with other essential protein and lipid molecules to dynamically regulate ICBs and the sequence of actions where ELs are required in spermatogenesis. In addition to the defective spermatogenesis, perinatal death, and growth retardation reported in this study, other abnormalities were also observed in the Far1 KO mice such as metabolic defects in adult mice and neuromuscular defects in aged mice. Therefore, these mice provide a valuable new model to investigate the physiological functions of ELs in different tissues and pathophysiology of EL deficiency in human diseases.

Supplementary Material

Refer to Web version on PubMed Central for supplementary material.

ACKNOWLEDGMENTS

This work is supported by research grants from the National Institute of Diabetes and Digestive and Kidney Diseases 1R01DK110314 to X. C. and the National Institute of Child Health and Human Development 1R01HD105944-01A1 to Z. Z. We thank Wei Li and Jihong Wang for their technical assistance. The Microscopy, Imaging, and Cytometry Resources Core are supported, in part, by NIH Center grant P30 CA22453 to the Karmanos Cancer Institute and R50 CA251068 to Dr. Moin. We thank the Wellcome Trust Sanger Institute Mouse Genetics Project and its funders for providing the mutant mouse line.

DATA AVAILABILITY STATEMENT

The data that support the findings of this study are available in the methods and/or supplementary material of this article.

REFERENCES

1. Braverman NE, Moser AB. Functions of plasmalogen lipids in health and disease. Biochim Biophys Acta. 2012;1822:1442–1452. [PubMed: 22627108]
2. Dean JM, Lodhi IJ. Structural and functional roles of ether lipids. Protein Cell. 2018;9:196–206. [PubMed: 28523433]
3. Dorninger F, Forss-Petter S, Wimmer I, Berger J. Plasmalogens, platelet-activating factor and beyond—ether lipids in signaling and neurodegeneration. Neurobiol Dis. 2020;145:105061. [PubMed: 32861763]
4. Messias MCF, Mecatti GC, Priolli DG, de Oliveira Carvalho P. Plasmalogen lipids: functional mechanism and their involvement in gastrointestinal cancer. Lipids Health Dis. 2018;17:41. [PubMed: 29514688]
5. Fallatah W, Schouten M, Yergeau C, et al. Clinical, biochemical, and molecular characterization of mild (nonclassic) rhizomelic chondrodysplasia punctata. J Inherit Metab Dis. 2021;44:1021–1038. [PubMed: 33337545]
6. Schooneveldt YL, Paul S, Calkin AC, Meikle PJ. Ether lipids in obesity: from cells to population studies. Front Physiol. 2022;13:841278. [PubMed: 35309067]
7. Kleiboeker B, Lodhi IJ. Peroxisomal regulation of energy homeostasis: effect on obesity and related metabolic disorders. Mol Metab. 2022;65:101577. [PubMed: 35988716]
8. Su XQ, Wang J, Sinclair AJ. Plasmalogens and Alzheimer's disease: a review. Lipids Health Dis. 2019;18:100. [PubMed: 30992016]
9. Cui W, Liu D, Gu W, Chu B. Peroxisome-driven ether-linked phospholipids biosynthesis is essential for ferroptosis. Cell Death Differ. 2021;28:2536–2551. [PubMed: 33731874]
10. Zou Y, Henry WS, Ricq EL, et al. Plasticity of ether lipids promotes ferroptosis susceptibility and evasion. Nature. 2020;585:603–608. [PubMed: 32939090]
11. Brites P, Motley AM, Gressens P, et al. Impaired neuronal migration and endochondral ossification in Pex7 knockout mice: a model for rhizomelic chondrodysplasia punctata. Hum Mol Genet. 2003;12:2255–2267. [PubMed: 12915479]
12. Rodemer C, Thai TP, Brugger B, et al. Inactivation of ether lipid biosynthesis causes male infertility, defects in eye development and optic nerve hypoplasia in mice. Hum Mol Genet. 2003;12:1881–1895. [PubMed: 12874108]
13. Liegel R, Chang B, Dubielzig R, Sidjanin DJ. Blind sterile 2 (bs2), a hypomorphic mutation in Agps, results in cataracts and male sterility in mice. Mol Genet Metab. 2011;103:51–59. [PubMed: 21353609]
14. Liegel RP, Ronchetti A, Sidjanin DJ. Alkylglycerone phosphate synthase (AGPS) deficient mice: models for rhizomelic chondrodysplasia punctate type 3 (RCDP3) malformation syndrome. Mol Genet Metab Rep. 2014;1:299–311. [PubMed: 25197626]
15. Gorgas K, Teigler A, Komljenovic D, Just WW. The ether lipid-deficient mouse: tracking down plasmalogen functions. Biochim Biophys Acta. 2006;1763:1511–1526. [PubMed: 17027098]
16. Rodemer C, Thai TP, Brugger B, Gorgas K, Just W. Targeted disruption of ether lipid synthesis in mice. Adv Exp Med Biol. 2003;544:355–368. [PubMed: 14713252]
17. O'Donnell L. Mechanisms of spermiogenesis and spermiation and how they are disturbed. Spermatogenesis. 2014;4:e979623. [PubMed: 26413397]
18. Griswold MD. Spermatogenesis: The commitment to meiosis. Physiol Rev. 2016;96:1–17. [PubMed: 26537427]
19. Walters JLH, Gadella BM, Sutherland JM, Nixon B, Bromfield EG. Male infertility: shining a light on lipids and lipid-modulating enzymes in the male germline. J Clin Med. 2020;9:327. [PubMed: 31979378]

20. Linn E, Ghanem L, Bhakta H, Greer C, Avella M. Genes regulating spermatogenesis and sperm function associated with rare disorders. Front Cell Dev Biol. 2021;9:634536. [PubMed: 33665191]
21. Beardsley A, Robertson DM, O'Donnell L. A complex containing alpha6beta1-integrin and phosphorylated focal adhesion kinase between Sertoli cells and elongated spermatids during spermatid release from the seminiferous epithelium. J Endocrinol. 2006;190:759–770. [PubMed: 17003277]
22. Wu S, Yan M, Ge R, Cheng CY. Crosstalk between Sertoli and germ cells in male fertility. Trends Mol Med. 2020;26:215–231. [PubMed: 31727542]
23. Mäkelä J-A, Toppari J. Spermatogenic cell syncytium. In: Skinner MK, ed. Encyclopedia of Reproduction. Academic Press; 2018:124–133.
24. Braun RE, Behringer RR, Peschon JJ, Brinster RL, Palmiter RD. Genetically haploid spermatids are phenotypically diploid. Nature. 1989;337:373–376. [PubMed: 2911388]
25. Greenbaum MP, Ma L, Matzuk MM. Conversion of midbodies into germ cell intercellular bridges. Dev Biol. 2007;305:389–396. [PubMed: 17383626]
26. Greenbaum MP, Iwamori T, Buchold GM, Matzuk MM. Germ cell intercellular bridges. Cold Spring Harb Perspect Biol. 2011;3:a005850. [PubMed: 21669984]
27. Otsuka K, Sawai-Ogawa M, Kihara A. Formation of fatty alcohols-components of meibum lipids-by the fatty acyl-CoA reductase FAR2 is essential for dry eye prevention. FASEB J. 2022;36:e22216. [PubMed: 35238077]
28. Cheng JB, Russell DW. Mammalian wax biosynthesis. I. Identification of two fatty acyl-Coenzyme A reductases with different substrate specificities and tissue distributions. J Biol Chem. 2004;279:37789–37797. [PubMed: 15220348]
29. Marsh KG, Arrieta A, Thuerauf DJ, Blackwood EA, MacDonnell L, Glembotski CC. The peroxisomal enzyme, FAR1, is induced during ER stress in an ATF6-dependent manner in cardiac myocytes. Am J Physiol Heart Circ Physiol. 2021;320:H1813–H1821. [PubMed: 33666503]
30. Honsho M, Fujiki Y. Plasmalogen homeostasis—regulation of plasmalogen biosynthesis and its physiological consequence in mammals. FEBS Lett. 2017;591:2720–2729. [PubMed: 28686302]
31. Honsho M, Abe Y, Fujiki Y. Plasmalogen biosynthesis is spatiotemporally regulated by sensing plasmalogens in the inner leaflet of plasma membranes. Sci Rep. 2017;7:43936. [PubMed: 28272479]
32. Honsho M, Asaoku S, Fukumoto K, Fujiki Y. Topogenesis and homeostasis of fatty acyl-CoA reductase 1. J Biol Chem. 2013;288:34588–34598. [PubMed: 24108123]
33. Matyash V, Liebisch G, Kurzchalia TV, Shevchenko A, Schwudke D. Lipid extraction by methyl-tert-butyl ether for high-throughput lipidomics. J Lipid Res. 2008;49:1137–1146. [PubMed: 18281723]
34. Zemski Berry KA, Murphy RC. Electrospray ionization tandem mass spectrometry of glycerophosphoethanolamine plasmalogen phospholipids. J Am Soc Mass Spectrom. 2004;15:1499–1508. [PubMed: 15465363]
35. Li W, Huang Q, Zhang L, et al. A single amino acid mutation in the mouse MEIG1 protein disrupts a cargo transport system necessary for sperm formation. J Biol Chem. 2021;297:101312. [PubMed: 34673028]
36. Lee KH, Park JH, Bunick D, Lubahn DB, Bahr JM. Morphological comparison of the testis and efferent ductules between wild-type and estrogen receptor alpha knockout mice during postnatal development. J Anat. 2009;214:916–925. [PubMed: 19538635]
37. Nakata H, Iseki S. Three-dimensional structure of efferent and epididymal ducts in mice. J Anat. 2019;235:271–280. [PubMed: 31148153]
38. Yuan S, Liu Y, Peng H, et al. Motile cilia of the male reproductive system require miR-34/miR-449 for development and function to generate luminal turbulence. Proc Natl Acad Sci U S A. 2019;116:3584–3593. [PubMed: 30659149]
39. de Rooij DG, Grootegoed JA. Spermatogonial stem cells. Curr Opin Cell Biol. 1998;10:694–701. [PubMed: 9914171]
40. Chen Y, Zheng Y, Gao Y, et al. Single-cell RNA-seq uncovers dynamic processes and critical regulators in mouse spermatogenesis. Cell Res. 2018;28:879–896. [PubMed: 30061742]

41. Green CD, Ma Q, Manske GL, et al. A comprehensive roadmap of murine spermatogenesis defined by single-cell RNA-Seq. Dev Cell. 2018;46:651–667.e10. [PubMed: 30146481]
42. Hermann BP, Cheng K, Singh A, et al. The mammalian spermatogenesis single-cell transcriptome, from spermatogonial stem cells to spermatids. Cell Rep. 2018;25:1650–1667.e8. [PubMed: 30404016]
43. Ernst C, Eling N, Martinez-Jimenez CP, Marioni JC, Odom DT. Staged developmental mapping and X chromosome transcriptional dynamics during mouse spermatogenesis. Nat Commun. 2019;10:1251. [PubMed: 30890697]
44. Greenbaum MP, Yan W, Wu MH, et al. TEX14 is essential for intercellular bridges and fertility in male mice. Proc Natl Acad Sci U S A. 2006;103:4982–4987. [PubMed: 16549803]
45. Honsho M, Asaoku S, Fujiki Y. Posttranslational regulation of fatty acyl-CoA reductase 1, Far1, controls ether glycerophospholipid synthesis. J Biol Chem. 2010;285:8537–8542. [PubMed: 20071337]
46. Komljenovic D, Sandhoff R, Teigler A, Heid H, Just WW, Gorgas K. Disruption of blood-testis barrier dynamics in ether-lipid-deficient mice. Cell Tissue Res. 2009;337:281–299. [PubMed: 19495798]
47. Brauns AK, Heine M, Todter K, Baumgart-Vogt E, Luers GH, Schumacher U. A defect in the peroxisomal biogenesis in germ cells induces a spermatogenic arrest at the round spermatid stage in mice. Sci Rep. 2019;9:9553. [PubMed: 31267012]
48. She ZY, Yang WX. Sry and SoxE genes: how they participate in mammalian sex determination and gonadal development? Semin Cell Dev Biol. 2017;63:13–22. [PubMed: 27481580]
49. Jameson SA, Lin YT, Capel B. Testis development requires the repression of Wnt4 by Fgf signaling. Dev Biol. 2012;370:24–32. [PubMed: 22705479]
50. Kim Y, Kobayashi A, Sekido R, et al. Fgf9 and Wnt4 act as antagonistic signals to regulate mammalian sex determination. PLoS Biol. 2006;4:e187. [PubMed: 16700629]
51. Jeays-Ward K, Hoyle C, Brennan J, et al. Endothelial and steroidogenic cell migration are regulated by WNT4 in the developing mammalian gonad. Development. 2003;130:3663–3670. [PubMed: 12835383]
52. Jorgez CJ, Seth A, Wilken N, Bournat JC, Chen CH, Lamb DJ. E2F1 regulates testicular descent and controls spermatogenesis by influencing WNT4 signaling. Development. 2021;148:dev191189. [PubMed: 33441379]
53. Iwamori T, Iwamori N, Ma L, Edson MA, Greenbaum MP, Matzuk MM. TEX14 interacts with CEP55 to block cell abscission. Mol Cell Biol. 2010;30:2280–2292. [PubMed: 20176808]
54. Lores P, Vernet N, Kurosaki T, et al. Deletion of MgcRacGAP in the male germ cells impairs spermatogenesis and causes male sterility in the mouse. Dev Biol. 2014;386:419–427. [PubMed: 24355749]
55. Cunto FD, Imarisio S, Camera P, Boitani C, Altruda F, Silengo L. Essential role of citron kinase in cytokinesis of spermatogenic precursors. J Cell Sci. 2002;115:4819–4826. [PubMed: 12432070]
56. Low SH, Li X, Miura M, Kudo N, Quinones B, Weimbs T. Syntaxin 2 and endobrevin are required for the terminal step of cytokinesis in mammalian cells. Dev Cell. 2003;4:753–759. [PubMed: 12737809]
57. Wang Y, Wang L, Iordanov H, et al. Epimorphin(−/−) mice have increased intestinal growth, decreased susceptibility to dextran sodium sulfate colitis, and impaired spermatogenesis. J Clin Invest. 2006;116:1535–1546. [PubMed: 16710473]
58. Fujiwara Y, Ogonuki N, Inoue K, et al. t-SNARE Syntaxin2 (STX2) is implicated in intracellular transport of sulfoglycolipids during meiotic prophase in mouse spermatogenesis. Biol Reprod. 2013;88:141. [PubMed: 23595907]
59. Osawa Y, Murata K, Usui M, et al. EXOC1 plays an integral role in spermatogonia pseudopod elongation and spermatocyte stable syncytium formation in mice. Elife. 2021;10:e59759. [PubMed: 33973520]
60. Carmena M, Riparbelli MG, Minestrini G, et al. Drosophila polo kinase is required for cytokinesis. J Cell Biol. 1998;143:659–671. [PubMed: 9813088]

61. Brill JA, Hime GR, Scharer-Schuksz M, Fuller MT. A phospholipid kinase regulates actin organization and intercellular bridge formation during germline cytokinesis. Development. 2000;127:3855–3864. [PubMed: 10934029]

62. Giansanti MG, Farkas RM, Bonaccorsi S, et al. Genetic dissection of meiotic cytokinesis in Drosophila males. Mol Biol Cell. 2004;15:2509–2522. [PubMed: 15004238]

63. Russell LD, Vogl AW, Weber JE. Actin localization in male germ cell intercellular bridges in the rat and ground squirrel and disruption of bridges by cytochalasin D. Am J Anat. 1987;180:25–40. [PubMed: 3310595]

64. Rabionet M, Bayerle A, Jennemann R, et al. Male meiotic cytokinesis requires ceramide synthase 3-dependent sphingolipids with unique membrane anchors. Hum Mol Genet. 2015;24:4792–4808. [PubMed: 26045466]

65. Zadravec D, Tvrdik P, Guillou H, et al. ELOVL2 controls the level of n-6 28:5 and 30:5 fatty acids in testis, a prerequisite for male fertility and sperm maturation in mice. J Lipid Res. 2011;52:245–255. [PubMed: 21106902]

66. Fujimoto H, Tadano-Aritomi K, Tokumasu A, et al. Requirement of seminolipid in spermatogenesis revealed by UDP-galactose: ceramide galactosyltransferase-deficient mice. J Biol Chem. 2000;275:22623–22626. [PubMed: 10801776]

67. Honke K, Hirahara Y, Dupree J, et al. Paranodal junction formation and spermatogenesis require sulfoglycolipids. Proc Natl Acad Sci U S A. 2002;99:4227–4232. [PubMed: 11917099]

68. da Silva TF, Eira J, Lopes AT, et al. Peripheral nervous system plasmalogens regulate Schwann cell differentiation and myelination. J Clin Invest. 2014;124:2560–2570. [PubMed: 24762439]

69. Perez MA, Magtanong L, Dixon SJ, Watts JL. Dietary lipids induce ferroptosis in *Caenorhabditis elegans* and human cancer cells. Dev Cell. 2020;54:447–454.e4. [PubMed: 32652074]

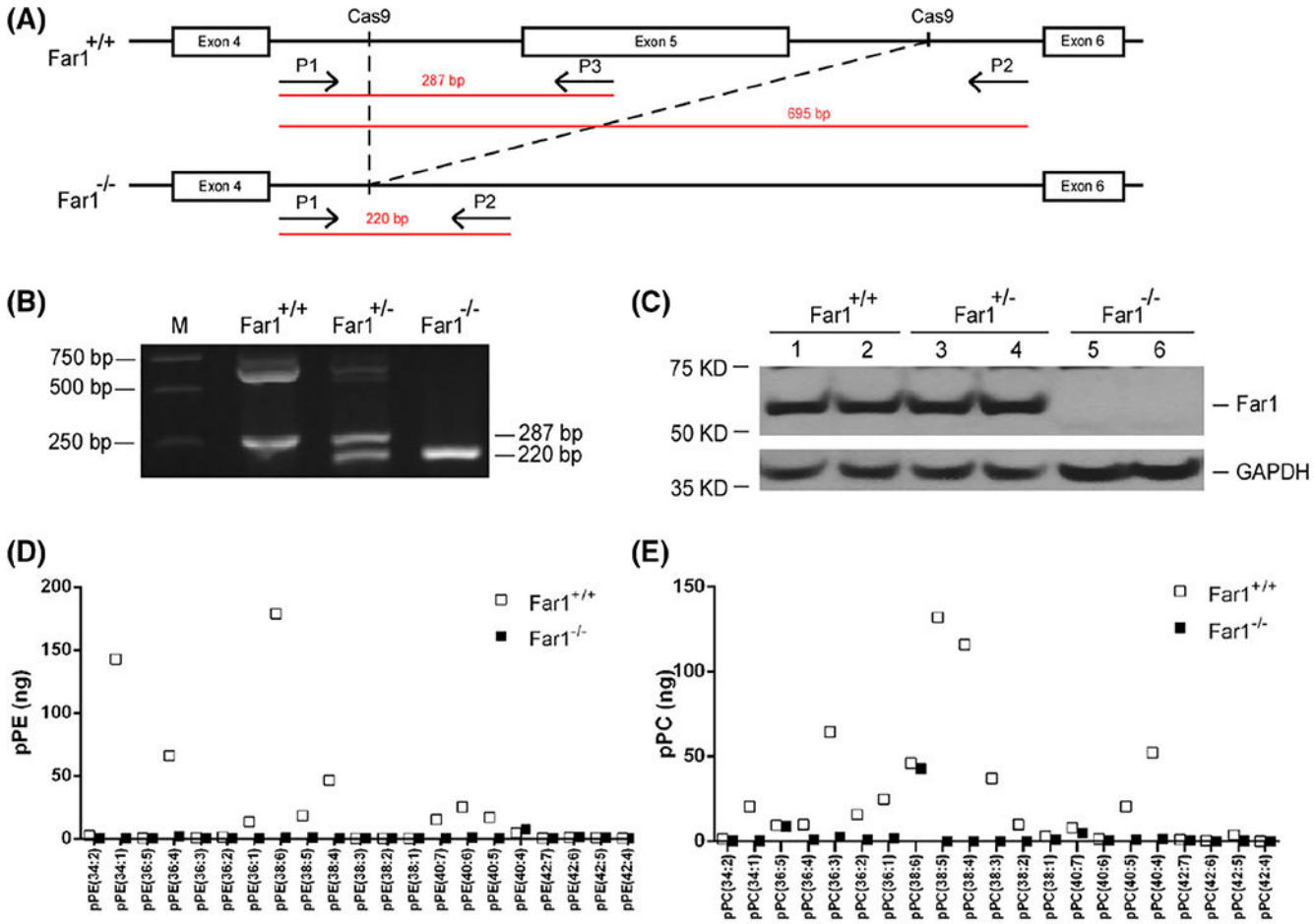

FIGURE 1.

Generation and validation of the Far1 knockout mice. (A) Four sgRNAs were used to target the intron sequences flanking the exon 5 of Far1 gene. Three primers were designed to validate the desired removal of the entire exon 5. (B) A representative genotyping PCR result to confirm the CRISPR/Cas9-mediated deletion of 475 bp. (C) Representative western blot result of Far1 protein in the testis ($n = 4$ in each genotype). Targeted lipidomic analyses of plasmalogen PE (pPE) (D) and plasmalogen PC (pPC) (E) in WT and Far1 KO mice.

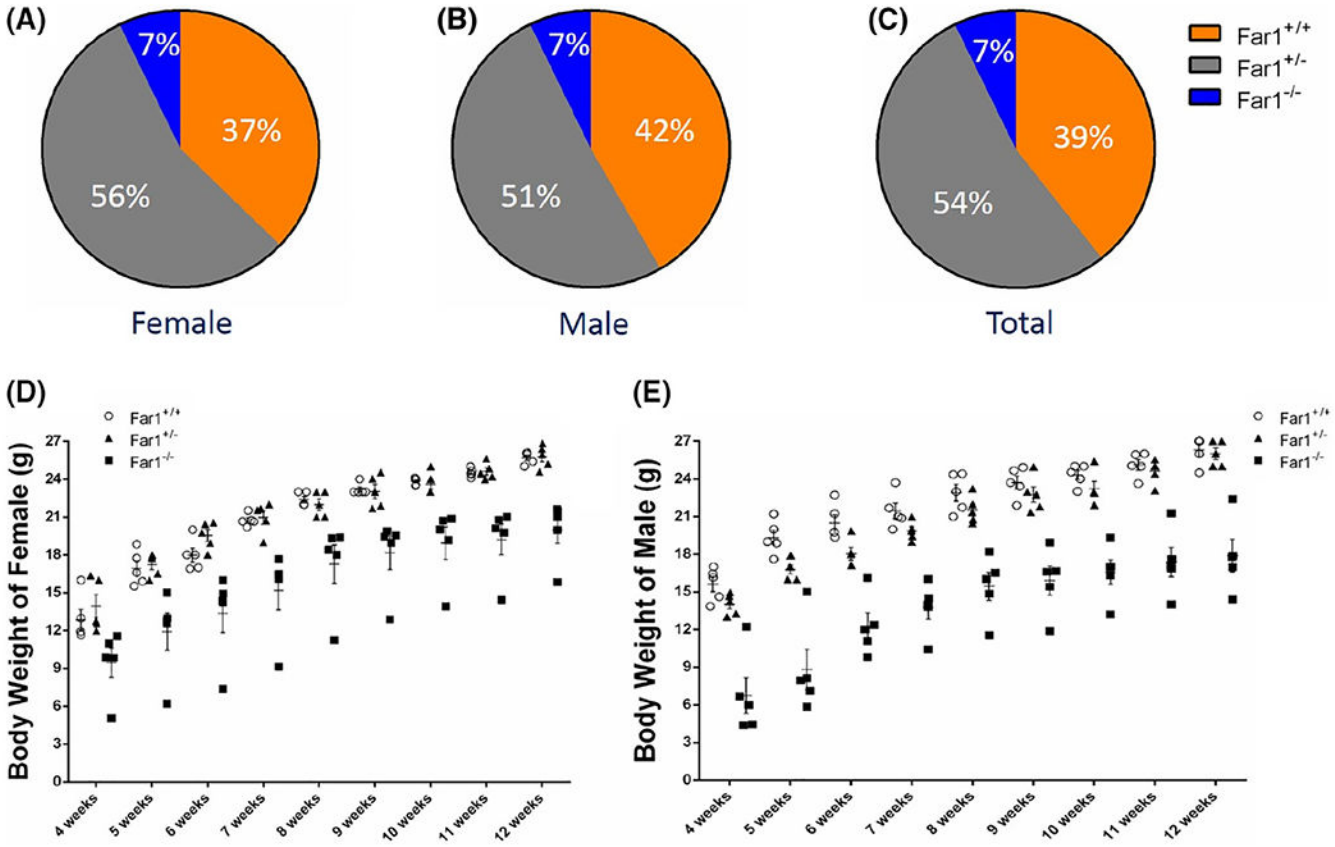

FIGURE 2.

Homozygous Far1 KO mice were subviable and displayed growth retardation. Genotype distribution was plotted separately for the female offspring (A), the male offspring (B), or combined (C) as the observed frequency (in percentage) of wild type, heterozygous, and homozygous genotype. The growth curves of the female (D) or male (E) offspring in each genotype ($n = 5$).

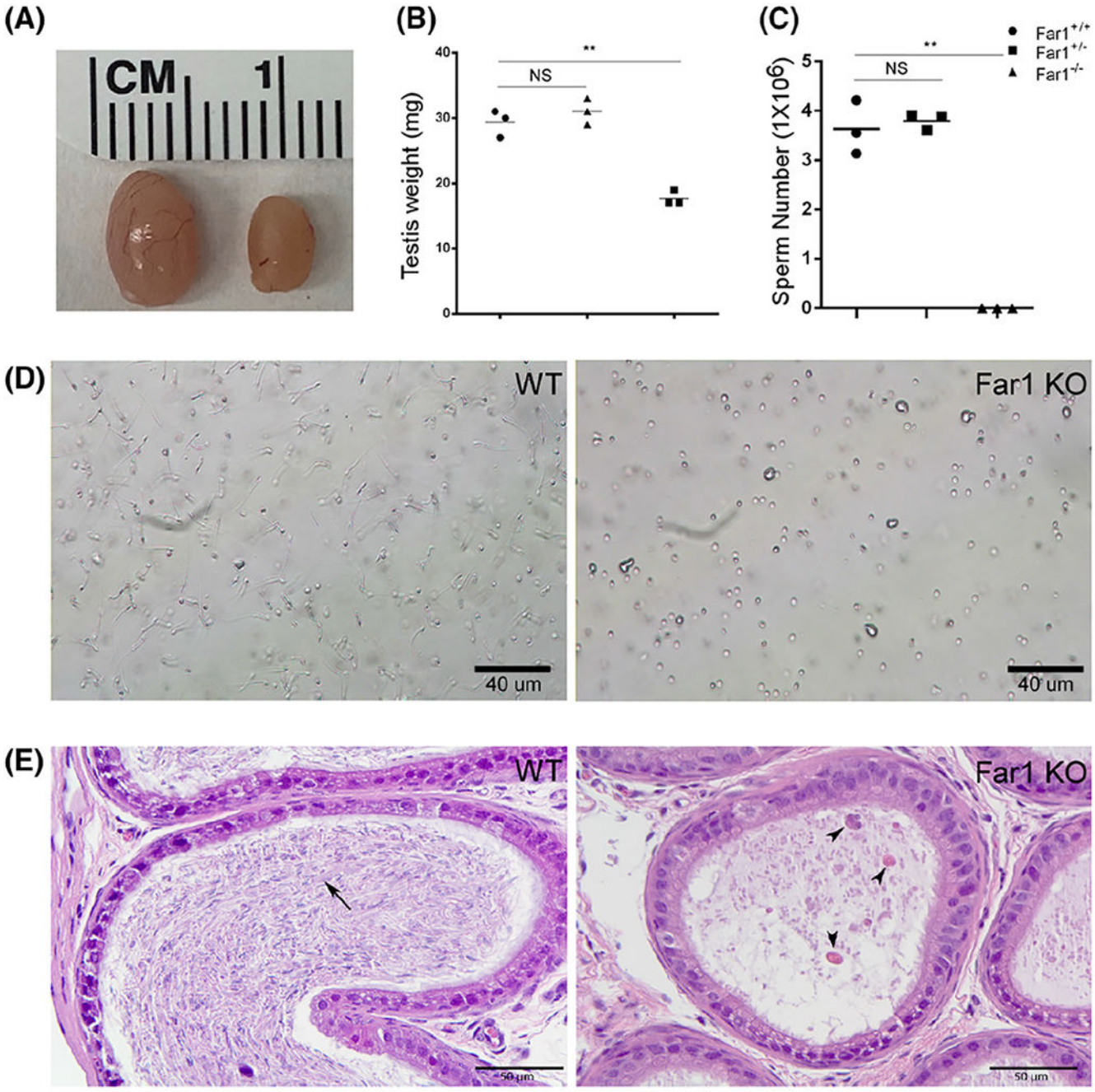

FIGURE 3.

Homozygous Far1 KO male mice produced no sperm. The testes of adult Far1 KO mice at 4 months appeared smaller (A) and weight less than the heterozygous and wild type (WT) mice (B). When sperms were released from the epididymis and counted under a microscope, there was no sperm found in the KO mice (C). A representative bright field image was presented for the wild type (D, *left*) and the KO mouse (D, *right*) respectively. H&E staining of the epididymis cross-section was shown in (E). On the left is the WT cauda epididymis showing a lumen filled with normal sperm head and long tails (arrow). On the right is

the Far1 KO cauda epididymis with a lumen containing cellular debris and round bodies (arrowheads), but no normal spermatozoa. Bars = 40 μm (D), and 50 μm (E). $^{**}p < .01$ vs. the control group; $n = 3$ biological repeats/group.

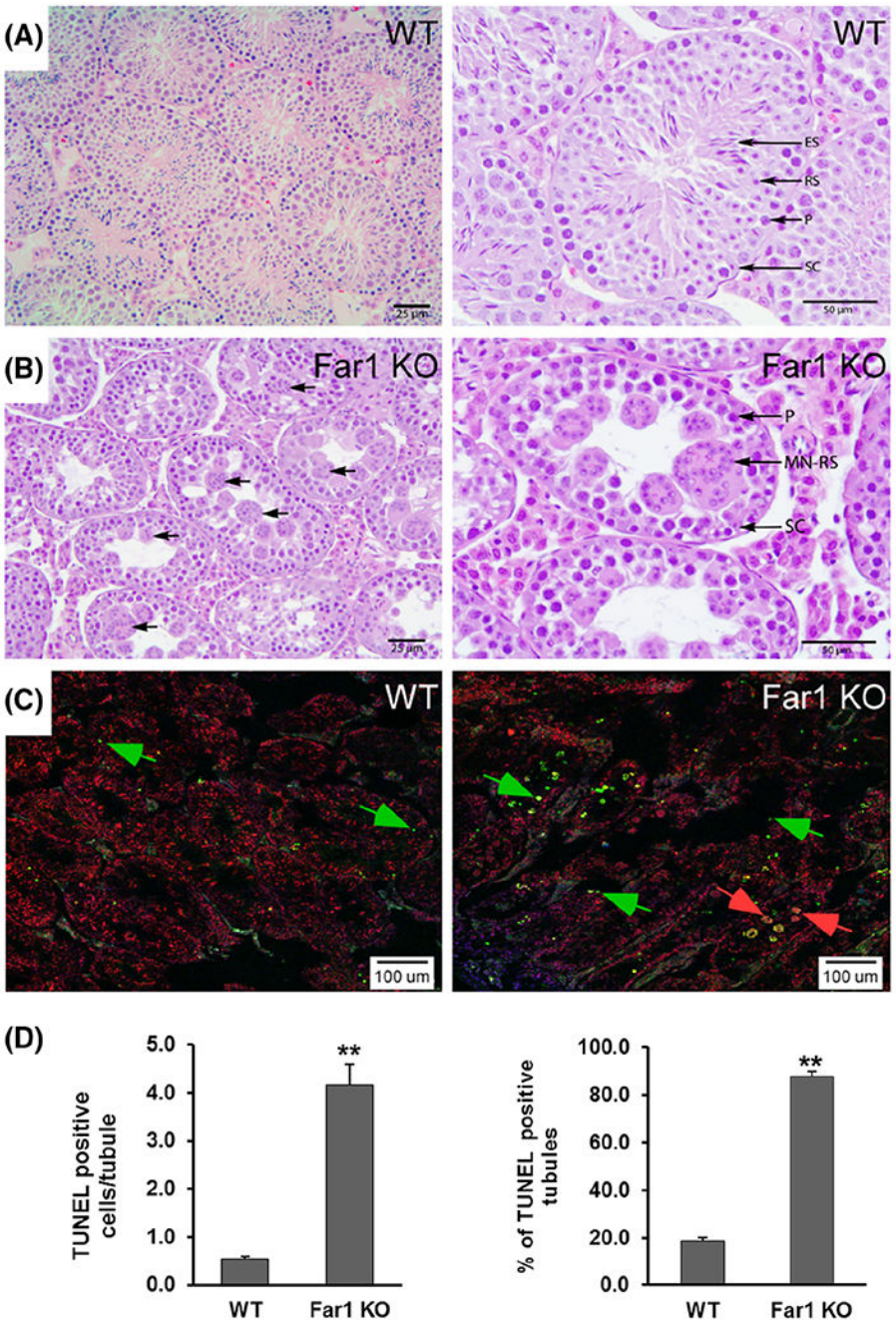

FIGURE 4.

Homozygous Far1 KO mice had disrupted spermatogenesis, very large multinucleated giant cells, and massive germ cell apoptosis. H&E staining of the WT (A *left*, 20×, *right*, 40×) and KO (B *left*, 20×, *right*, 40×) testis cross sections. In B, on the left is a low magnification of the Far1 KO testis showing numerous multinucleated giant cells, some containing over 30 round germ cell nuclei in a 5 μm section (arrows). On the right is a higher magnification of the Far1 KO testis showing numerous multinucleated giant cells with round spermatids (MN-RS) lining the tubule lumen, some reaching greater than 50 μm in diameter. Normal

pachytene spermatocyte nuclei (P) and Sertoli cells (SC) are noted closer to the basement membrane. Bars = 25 and 50 μm. TUNEL staining (green) showed massive germ cell apoptosis in Far1 KO (C, *right*) but not WT testis (C, *left*). The nuclei were stained with DAPI (blue) and propidium iodide was in red. Scale bar = 40 μm. Quantification of the numbers of apoptotic cells per seminiferous tubule and the percentage of TUNEL-positive tubules were shown in (D). $^{**}p < .01$ Far1 KO vs. WT, $n = 3$ per genotype.

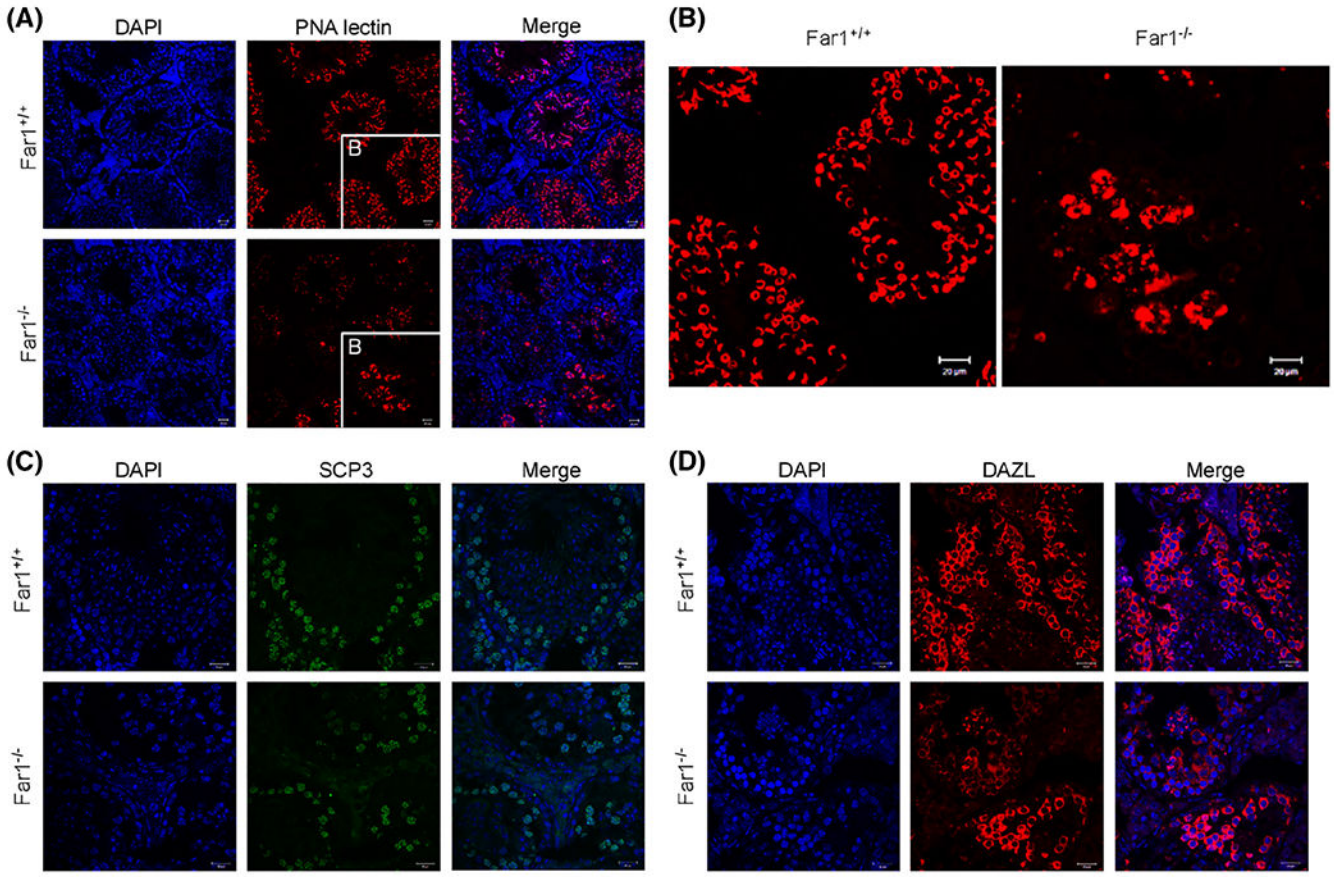

FIGURE 5.

Immunofluorescent staining of cell type-specific markers in WT and Far1 KO testes. To understand the cell-type specific defect of spermatogenesis, specific markers were used in the immunofluorescent staining of the WT and KO testis. PNA lectin was in red (A) with higher magnification insets (B), SCP3 in green (C), and DAZL in red (D). The nuclei were stained with DAPI (blue). Scale bar = 40 μm (A, C, D) and 20 μm (B).

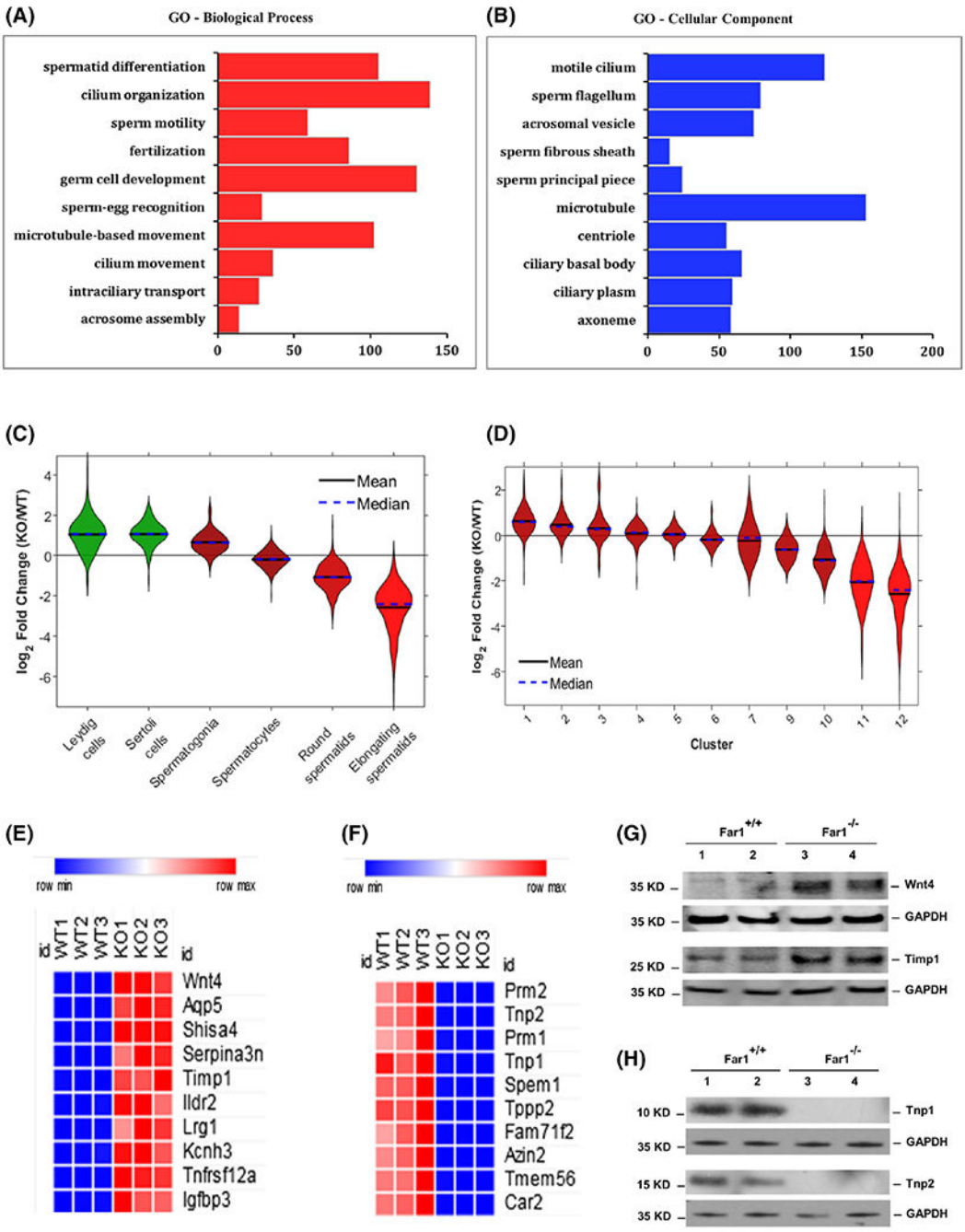

FIGURE 6.

RNA sequencing and bioinformatics analysis identified cell type-specific and stage-specific requirements of ether lipids in spermatogenesis. RNA sequencing and differential analysis were performed to compare the testicular gene expressions between WT and KO mice (n = 3 in each group). Gene Ontology (GO) analyses of the differentially expressed genes showed that among the top 10 most downregulated GO Biological Processes (A) and GO Cellular Components (B) were those related to spermatid differentiation, sperm motility, and fertilization. When comparing our results with the specific markers published in a recent

scRNASeq study,[41] cell type-specific (C) and stage-specific (D) changes in spermatogenesis were unveiled. D: germ cell cluster 1 included both undifferentiated and differentiating spermatogonia cells. 2–3 represented transient cellular states from spermatogonia to early spermatocytes. 4–8 correlated with various stages of spermatocytes. 9–11 were enriched with round spermatids and cluster 12 with elongated spermatids. There was no unique marker for cluster 8.[41] (E) a heatmap highlighted the top-ranked upregulated genes in Far1 KO testis. (F) a heatmap highlighted the top-ranked downregulated genes in Far1 KO testis. (G) western blot analysis from two mice in each group confirmed the dramatic increase of Wnt4 and Timp1 protein expression. (H) western blot analysis from two mice in each group confirmed the dramatic decrease of Tnp1 and Tnp2 protein expression. GAPDH was used as the load control in all experiments.

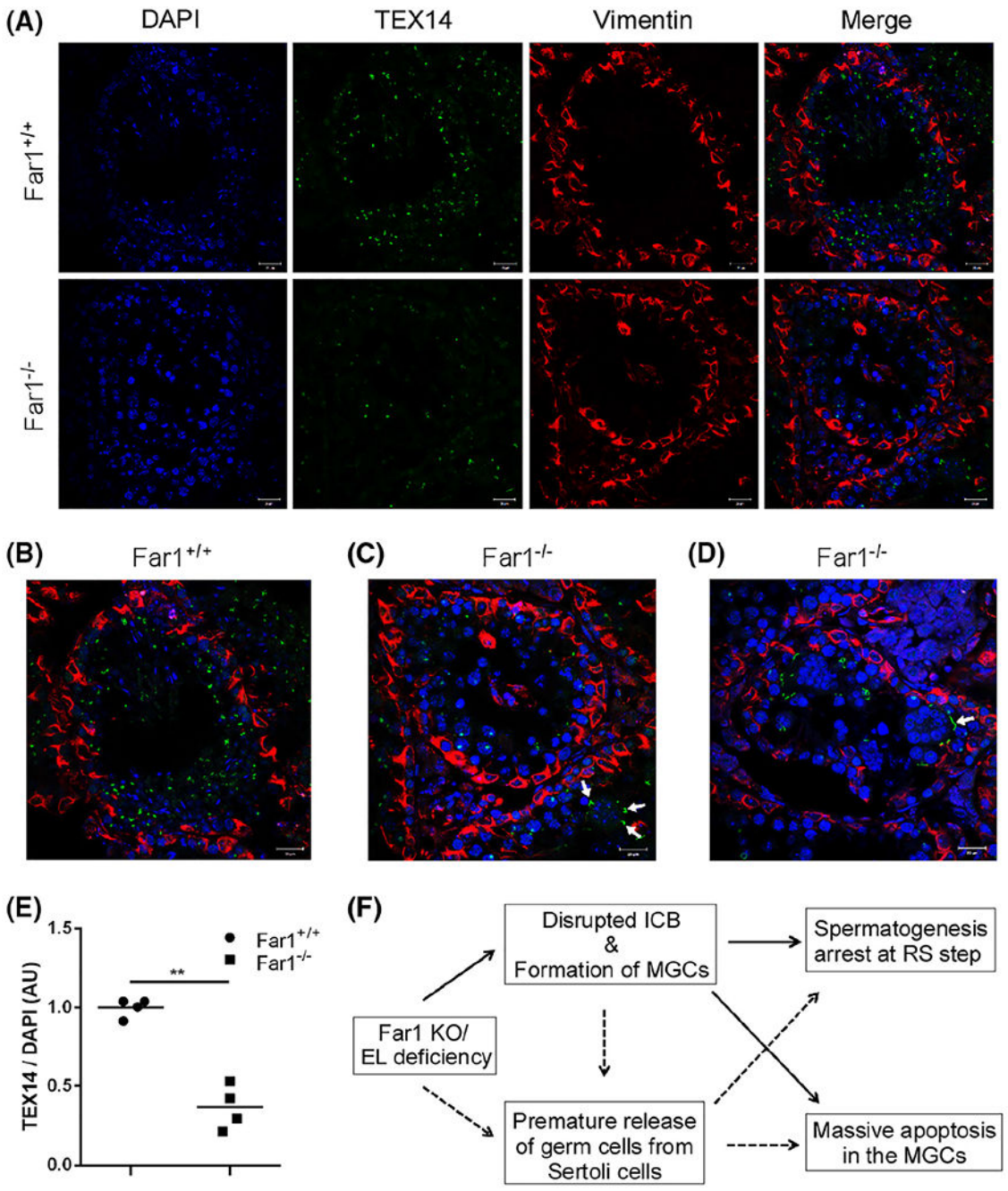

FIGURE 7.

Intercellular bridges were disrupted in the homozygous Far1 KO mice. (A) immunofluorescent staining of intercellular bridge marker TEX14 (green) showed many puncta in the wild type but not in the KO testis. Sertoli cell marker, vimentin was shown in red. Higher magnification insets were shown in (B, C, and D). The nuclei were stained with DAPI (blue). Scale bar = 40 μm. Patchy Tex14 staining was observed on the multinucleated giant cell membrane in Far1 KO testis (C, D, white arrows). Quantitative analysis of intercellular bridges (TEX14/DAPI) for both WT and Far1 KO mouse testis was shown

in (E). A summary of spermatogenesis deficiencies in Far1 KO testis is shown in (F). The solid arrows indicate the affected pathways supported by this study and the dashed arrows indicate the additional pathways which could also be affected. $^{**}p < .01$ vs. the control group; $n = 4$ biological repeats/group.